



The Horizontal Sonocapillary Effect in Ultrasonic-Assisted Soldering

Numerical simulations and experiments were conducted to study the acoustic pressure of the liquid solder

BY S. CHEN, Z. XU, Z. LI, Z. MA, L. MA, AND J. YAN

Abstract

In this work, the horizontal sonocapillary effect in ultrasonic-assisted soldering was investigated via numerical simulations and experiments. The numerical simulation results indicated that acoustic pressures in the liquid solder exhibited distinct sinusoidal features with negative offsets, forming a negative average acoustic pressure. When the ultrasonic vibrations were transmitted to the lower substrate in the joint clearance, the average acoustic pressures decreased from the acoustic pressure center to the filling front, forming a negative acoustic pressure gradient in the horizontal direction. As a result, the solder was sucked into the joint clearance by a large negative acoustic pressure. This sonocapillary effect was verified with experiments. In the calculation model, a high ultrasonic amplitude, a small joint clearance width, and a high base material stiffness increased the acoustic pressure and its average difference on the horizontal direction in the solder, which further improved the driving force of the sonocapillary effect. However, the wetting angle had a small influence on the sonocapillary effect.

Keywords

- Sonocapillary Effect
- Acoustic Pressure
- Velocity
- Filling Mechanism

Introduction

It is well known in the field of traditional soldering that capillary filling depends on the wetting of the liquid solder to the substrate (Refs. 1–4). However, recent reports have shown that under ultrasonic assistance, liquid solder is able to infiltrate a horizontal joint clearance at a high velocity without wetting the substrate (Refs. 5–8). This capillary filling promoted by ultrasonication is called the sonocapillary effect. In previous work by the authors, a zinc-aluminum (Zn-Al) alloy filled a soldering joint clearance before the break of the oxide layer (Al_2O_3) on an $Al_2O_3/6061$ Al composite (Ref. 5). Because the Zn-Al alloy could not wet the Al_2O_3 , the sonocapillary effect occurred without wetting the substrate. Chen et al. (Ref. 6) used the sonocapillary effect to solder aluminum-titanium (Al-Ti) dissimilar alloys, and the infiltration time was only several seconds. Recently, this effect was applied to several porous materials to drive the liquid metal to fill the pores (Ref. 8).

Despite the widespread application of ultrasonic-assisted soldering, little attention has been focused on the mechanism of the sonocapillary effect in this method. However, discussions about the use and mechanism of this effect in some other fields have been reported — such as in the extraction of food and natural products (Refs. 9–11), metal treatment (Ref. 12), oil recovery (Ref. 13), or chips (Refs. 14–16) — as well as general discussions without a specific application background (Refs. 17–19). Several investigations found that surface acoustic waves are the main reason that the sonocapillary effect occurs (Refs. 14–16, 20). The surface acoustic wave can cause acoustic streaming (Ref. 14) and atomization (Ref. 20), which drive the liquid flow. Many researchers have suggested that cavitation is the main mechanism of the sonocapillary effect (Refs. 17, 18, 21, 22).

Malykh et al. (Ref. 17) as well as Dezhkunov and Leighton (Ref. 18) found that the driving pressure was the highest with

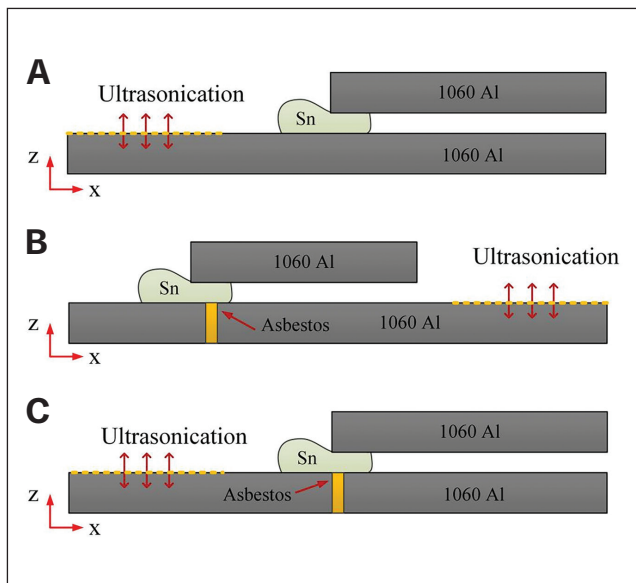


Fig. 1 – Schematic of the filling with different ultrasonic application locations: A – On the entire lower substrate (mode I); B – on the lower substrate inside (mode II); C – outside the joint clearance (mode III).

a cluster of cavitation bubbles. Tamura and Hatakeyama (Ref. 22) suggested that the radiation pressure caused by cavitation at the tube's open end plays a key role in the liquid pressurization. Hu et al. (Ref. 23) proposed that changes in the cohesive forces between the liquid molecules and adsorption forces between the liquid molecules and capillary tubes activate the sonocapillary effect. Another mechanism of the sonocapillary effect was reported by Rozina (Ref. 19), who suggested that gas dissolution in a sealed tube brings about a pressure difference inside and outside the tube. As a result, the liquid is pushed into the tube. The limitation of this theory is that it cannot explain the sonocapillary effect in open channels.

Due to the fast-filling speed of solder during soldering with the assistance of ultrasonication (Refs. 5–8), this study focuses on the mechanism of the horizontal sonocapillary effect. It also focuses on the change in the liquid acoustic pressure without considering the cavitation effect. In previous work, the authors demonstrated that the cavitation effect is not necessary in the sonocapillary process (Ref. 24). Based on the observations of sonocapillary morphology, numerical simulations were carried out to explain the experimental results. Ansys software was applied to analyze the vibration

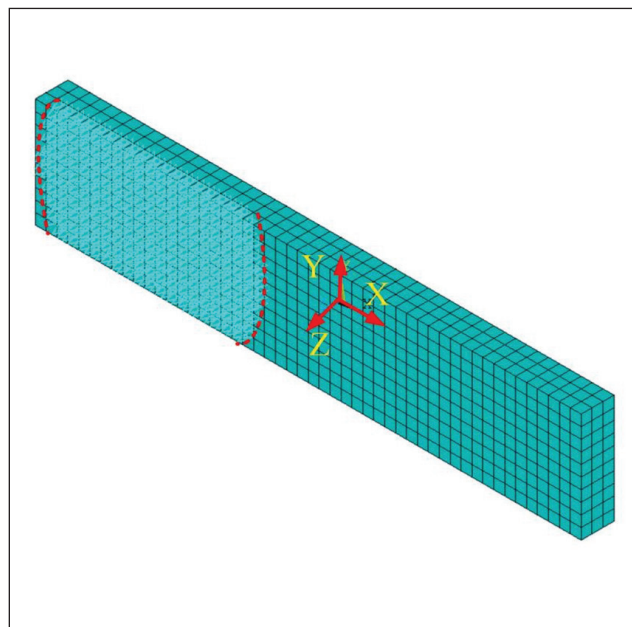


Fig. 2 – Simulation model of the vibrations on the lower plate.

of the substrate. Then, vibrations were introduced into Ansys Fluent software to calculate the acoustic pressure distribution. The infiltration velocity within one acoustic cycle was studied, and the influences of the ultrasonic amplitude, joint clearance width, wetting angle, and property of the base material on the sonocapillary behavior were analyzed.

Experimental and Numerical Methods

Experimental

A schematic diagram of the sonocapillary effect with different ultrasonic application locations is shown in Fig. 1. The ultrasonic horn was placed on the lower plate where the yellow dotted line is shown. The arrows refer to the direction of the excitation vibration. The substrates selected for this work were 1060 Aluminum Alloy. The solder was pure tin (Sn) with a melting point of 232°C (449.6°F), and the test temperature was set to 250°C (482°F). The ultrasound was applied after reaching the soldering temperature. In mode I, the substrates had dimensions of 50 × 10 × 3 mm (1.968

Table 1 – Boundary Conditions of the Simulation Process

Location	Lower Surface	Four-Sided Surfaces	Upper Surface
Boundary conditions	$U_x = 0$ $U_y = 0$	Unrestrained	U_z

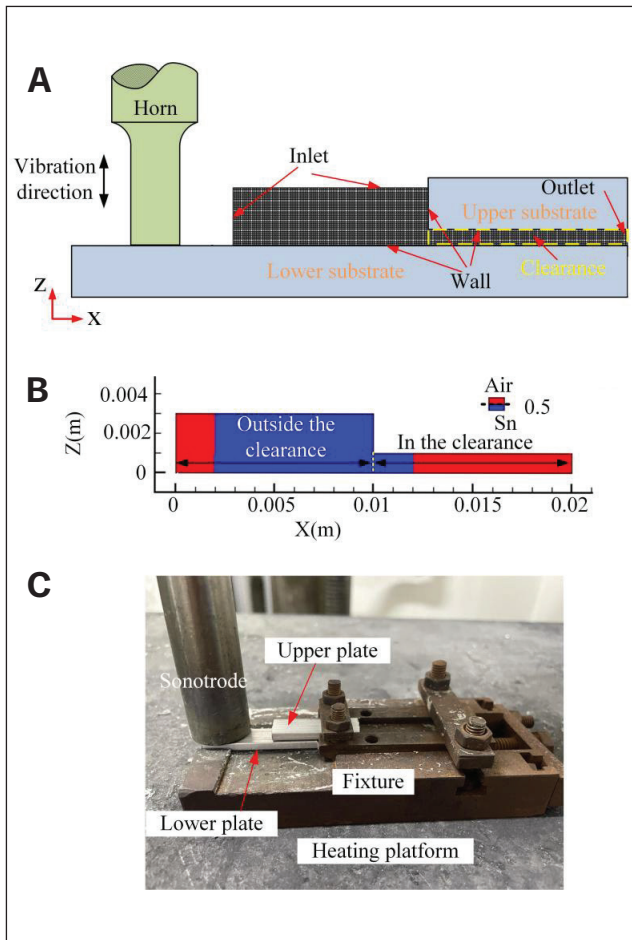


Fig. 3 – Calculation of sonocapillary effect: A – Meshing model; B– initial state; C – experimental setup.

$\times 0.393 \times 0.118$ in.) and $25 \times 10 \times 3$ mm ($0.984 \times 0.393 \times 0.118$ in.). Ultrasonication was applied on the entire lower substrate. In mode II, the dimensions of the substrates were $15 \times 10 \times 3$ mm ($0.590 \times 0.393 \times 0.118$ in.), $35 \times 10 \times 3$ mm ($1.377 \times 0.393 \times 0.118$ in.), and $25 \times 10 \times 3$ mm. In mode III, the dimensions of all substrates were $25 \times 10 \times 3$ mm. In modes II and III, the ultrasonic excitation was separately applied on the lower substrate inside and outside the joint clearance, respectively. The joint clearance size was 1 mm (0.039 in.), and it was controlled by a feeler gauge. The ultrasonic time and amplitude were set at 4 s and $5 \mu\text{m}$, respectively. Sound-resistant asbestos was used to hinder the ultrasonic transmission. The asbestos was fixed between the two sections of the lower plate. Both the metal substrates and the solder were first cleaned using silicon-carbide (SiC) emery paper, after which they were ultrasonically cleaned in acetone for 15 min. A self-designed ultrasonication system, UPM-UP-1010A01, with an ultrasonic frequency of 20 kHz was applied. The TC 4 sonotrode had a diameter of 20 mm (0.787 in.). Three samples were prepared in each condition.

After soldering, the joint was cooled to room temperature in air and cut along the central line. The cross section was then ground and polished. The microstructures of the joints were analyzed using a Zeiss scanning electron microscope.

Numerical

A simulation model of the vibrations on the lower substrate excited by ultrasonication was developed using Ansys software – Fig. 2. The boundary conditions of the simulation process are presented in Table 1. Ultrasonication was applied on the left side of the substrate, as marked with the red dotted lines.

U_z represents the ultrasonic vibrations in the Z-direction. They are described as follows:

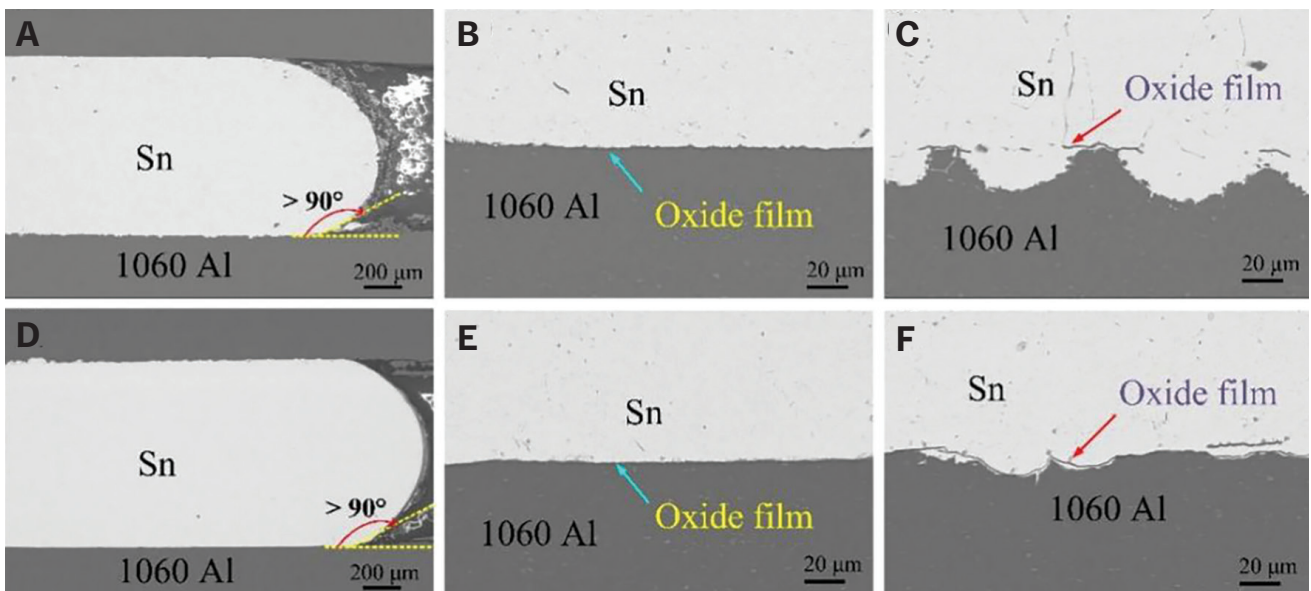


Fig. 4 – Sonocapillary morphologies and microstructures of the Sn/1060 Aluminum Alloy interface: A – Wetting angle; B – interface near the filling front; C – interface away from the filling front in mode I; D – wetting angle; E – interface near the filling front; F – interface away from the filling front in mode II.

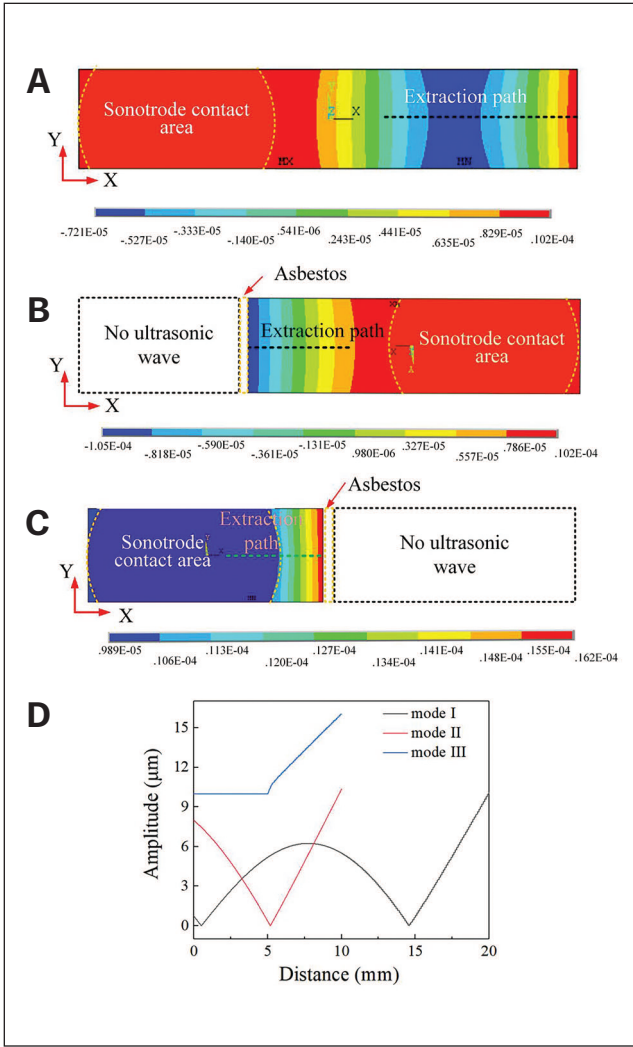


Fig. 5 – Vibration distributions in the Z-direction on the lower substrate: A – Mode I; B – mode II; C – mode III; D – along the extraction path.

$$U_z = U_0 \cdot \sin(2\pi ft) \quad (1)$$

where U_0 is the ultrasonic vibration amplitude, f is the ultrasonic frequency, and t is the time. There are three different substrates used in the simulation model: 1060 Al, 5056 Al, and Fe36Ni. Their elastic moduli are shown in Table 2.

Table 2 – Elasticity Moduli of Different Substrates

Material	1060 Al	5056 Al	Fe36Ni
Elasticity Modulus (GPa)	68.9	71.7	142.0

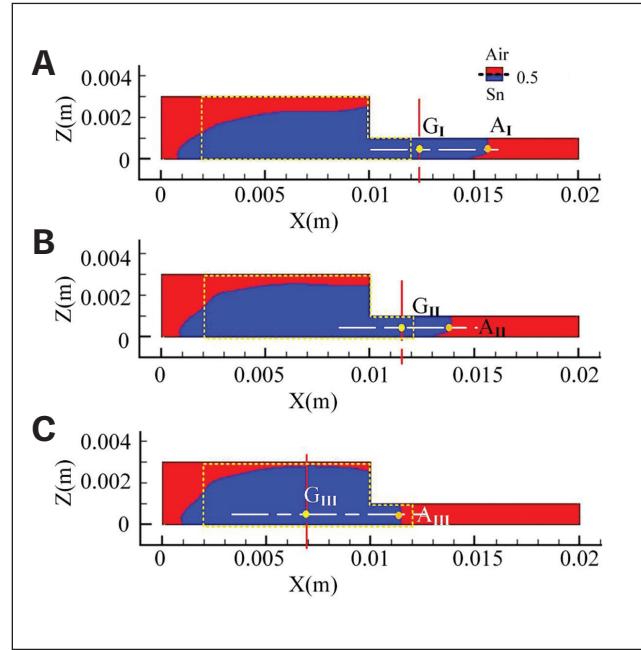


Fig. 6 – Sonocapillary states of different modes at 5 ms: A – Mode I; B – mode II; C – mode III.

The sonocapillary conditions were analyzed using the Fluent software. The simulation model is shown in Fig. 3. It was established in 2D space based on an ideal condition. The turbulent flow of the liquid was set to a K-epsilon model. The length and width of the joint clearance were set as 10 and 1 mm, respectively. The left 10 mm was outside the joint clearance, and the right 10 mm was inside the joint clearance – Fig. 3B. The sonocapillary effect did not rely on the wetting condition. For simplification, the initial shape of the liquid in the joint clearance was simplified to be rectangular. The boundary settings of the wall, pressure inlet, and pressure outlet are marked in Fig. 3. The left and upside gas-liquid interfaces were selected as the pressure inlet interface with a barometric pressure. The interfaces of the liquid metal and solid plate were defined as the wall, where the liquid cannot pass. The right boundary of the joint clearance was chosen to be the pressure outlet. The vibrations were applied on the upper surface of the lower plate via a user-defined function. This function was a series of C programs based on the vibrations varied with time and location. For example, 40 points were selected along the extraction path for mode I. The displacement of each surface point followed a function with the following form:

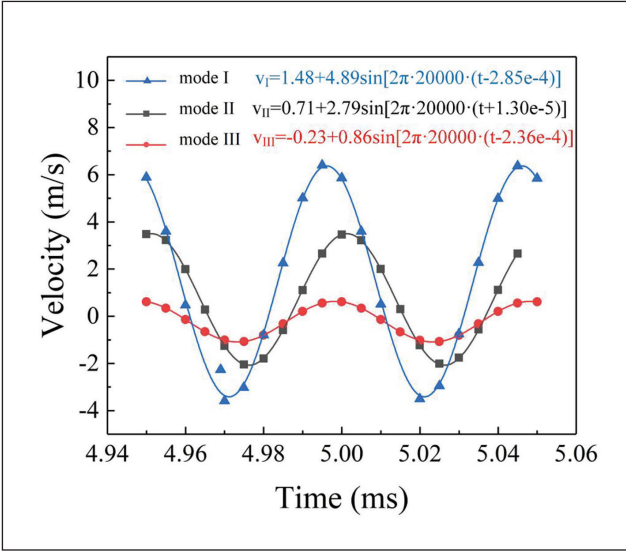


Fig. 7 – Sonocapillary velocity at the filling front of point A from 4.95 to 5.05 ms.

$$U'_z = U'_0 \sin(2\pi ft) \quad (2)$$

where U'_z is the vibration displacement at the moment of t , U'_0 is the vibration amplitude, and f is the vibration frequency. Different points had different U'_0 , which could be calculated from the model in Fig. 2. The roughness of the wall, wetting angle of the solder on the substrate, ultrasonic amplitude, and ultrasonic frequency were set to be $1.5 \mu\text{m}$, 130 deg ,

$5 \mu\text{m}$, and 20 kHz , respectively, which were the same as those in the sonocapillary experiments. In Fig. 3B, the red area represents air, and the blue area corresponds to liquid metal. Figure 3C shows the experimental setup used for the sonocapillary effect.

Results

Sonocapillary Morphologies for Different Ultrasonication Application Modes

Experiments were carried out to test the sonocapillary effect with different ultrasonication application locations. The wetting angles and microstructures of the pure Sn/1060 Aluminum Alloy interface are shown in Fig. 4. The filling lengths in modes I and II were 12.9 and 10 mm (0.507 and 0.393 in.), respectively. It can be seen from Fig. 4A that the wetting angle of pure Sn on 1060 Aluminum Alloy was more than 90 deg , indicating that the solder did not wet the substrate. Compared with the Sn/1060 Aluminum Alloy interface away from the filling front in mode I (Fig. 4C), the interface near the filling front in Fig. 4B showed that the oxide film was intact. The composition of the oxide film on the 1060 Aluminum Alloy surface was examined in a previous work by the authors (Ref. 25). The oxide film away from the filling front broke due to the cavitation time being long enough. However, the oxide film near the filling front did not break because the cavitation time was short. This phenomenon was also reported in previous works by the authors (Refs. 5, 6). Similar results were found for mode II.

Table 3 – Pressure Function Parameters of Different Locations

P_u (Pa)	P_c (Pa)	P_A (Pa)	f (Hz)
P_{uAI}	$-5.60\text{e}4$	$2.42\text{e}6$	20,000
P_{uGI}	$-4.38\text{e}4$	$9.05\text{e}6$	20,000
P_{uAII}	$-1.81\text{e}4$	$1.35\text{e}6$	20,000
P_{uGII}	$-1.12\text{e}4$	$4.29\text{e}6$	20,000
P_{uAIII}	$-1.96\text{e}3$	$2.12\text{e}5$	20,000
P_{uGIII}	$-3.66\text{e}3$	$2.17\text{e}6$	20,000

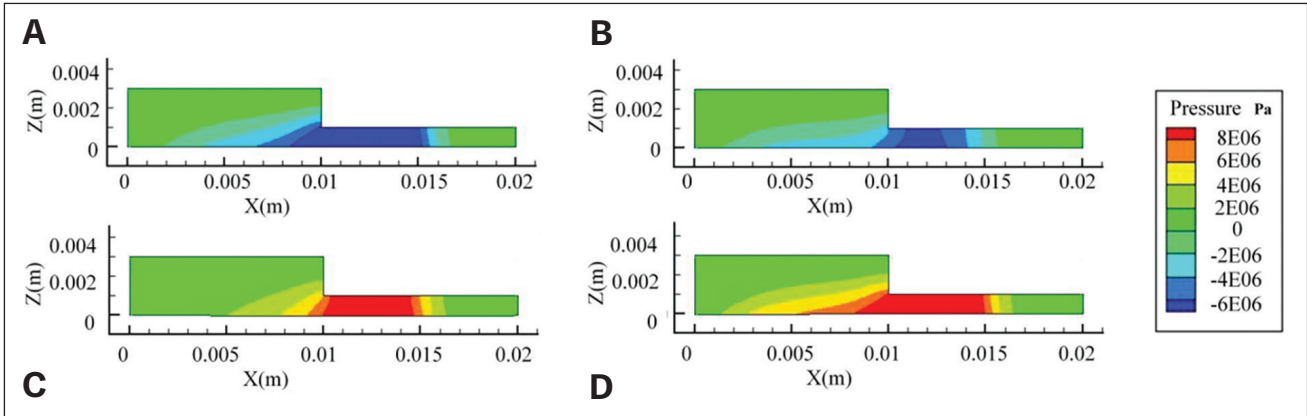


Fig. 8 – Alternating acoustic pressure within one acoustic cycle in mode I: A – 5010 μ s; B – 5020 μ s; C – 5030 μ s; D – 5040 μ s.

Additionally, the wetting angle was more than 90 deg (Fig. 4D), the oxide film near and far from the filling front had different morphologies (Figs. 4E, F), and the intact film was broken by the cavitation effect. The obtuse angle of the wetting front demonstrated that the sonocapillary effect occurred before the wetting process (the breaking of the oxide film), which was also reported in several other works (Refs. 5–7). The solder could wet the fresh Al metal but not the oxide film. This sonocapillary phenomenon cannot occur in traditional brazing. In mode III, the sonocapillary effect could not be realized.

Sonocapillary Mechanism

Figure 5 shows the vibration distribution on the lower plate under the ultrasonic excitation. It was acquired by a harmonic analysis. The color scale indicates the displacement of the surface points of the plate subjected to ultrasonic vibration. The displacement refers to the movements of these surface points. The displacement was 0 when the plate was kept at its original position. Figure 5 shows negative values when the surface points moved downward and positive values when the surface points moved upward. The vibration amplitude was the absolute value of the maximum displacement, which was 0 or a positive value. The vibration amplitude on the extraction path could represent the changes of vibrations of the plate surface points. Figure 5D shows the vibration amplitudes along the extraction paths. In mode I, the largest vibration amplitudes appeared on the right red region because of the reflection and superposition of the sound waves (Ref. 26). In mode II, the vibration amplitudes first decreased and then increased along the extraction path. However, the vibration amplitudes first remained at a certain level and then rose gradually in mode III.

The vibration on the lower plate was introduced to the computational fluid dynamics model via a user-defined function. It was a series of C programs based on the vibrations and locations curve. The simulation results at 5 ms are shown in Fig. 6. The yellow dotted line shows the initial state of the liquid solder. In mode I, the sonocapillary effect was the best, which was indicated by the longest filling length of nearly 0.004 m (0.157 in.) in the joint clearance. The sono-

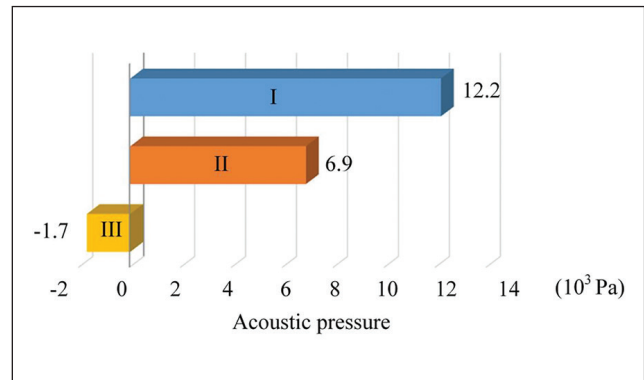


Fig. 9 – Difference of average acoustic pressure between points A and G for modes I–III.

capillary effect was also realized in mode II. However, the solder moved out of the joint clearance in mode III when the ultrasonication was only applied on the lower substrate outside the joint clearance. These results agreed with those in Fig. 4. The sonocapillary effect in mode I was the best, and no sonocapillary effect occurred in mode III.

We calculated the sonocapillary velocity at the filling front of point A (marked in Fig. 6) from 4.95 to 5.05 ms. Figure 7 shows the velocity variations of the three modes, which all exhibited sinusoidal features. Expressions of their fitted curves were acquired using Origin software. The velocity and time curves showed differences in amplitude and offset, which were the main parameters. In addition, the initial phases of the sinusoidal curves could be neglected due to the periodicity of the curves.

The average velocity of an acoustic cycle from 4.95 to 5.05 ms can be calculated via integration:

$$\bar{v} = \frac{1}{T} \int_0^T v dt \quad (3)$$

The average velocities at modes I–III were 1.48, 0.71, and -0.23 m/s, respectively.

Figure 8 presents the pressure in the liquid metal at mode I within one acoustic cycle. The pressure alternated between positive and negative values. The center of the acoustic pres-

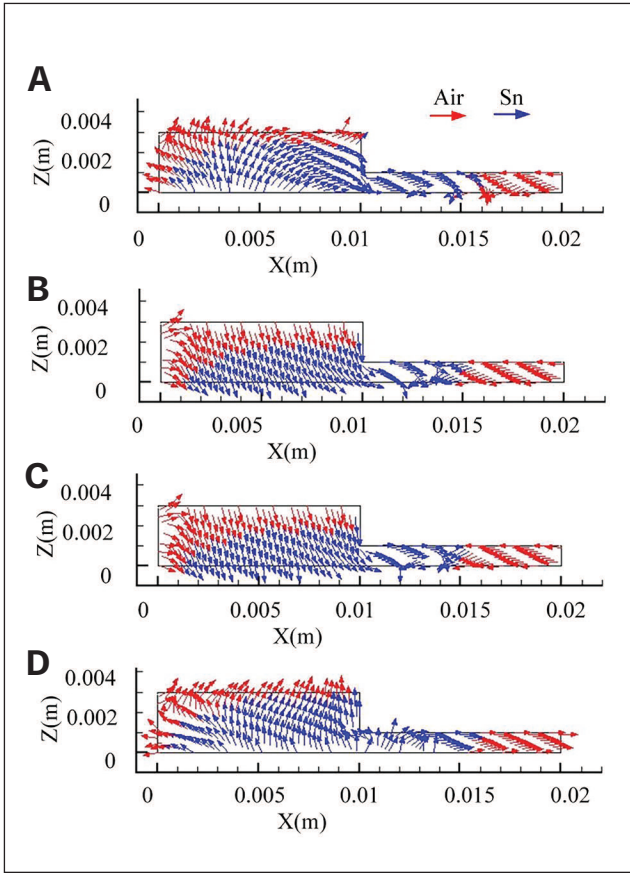


Fig. 10 – Velocity changes of solder and air within an acoustic cycle in mode I: A – 5010 μs ; B – 5020 μs ; C – 5030 μs ; D – 5040 μs .

sure was determined according to the distribution of acoustic contours in which the peak of the acoustic pressure amplitude was named point G. The pressure changed continuously from the center to the left and right liquid-gas interfaces.

Two representative points, namely the filling front A and the center of the acoustic pressure G, were selected to quantitatively show the relationship between the acoustic pressure and the ultrasonication application duration. The feature points are marked in Fig. 6. The relationship between acoustic pressure and time is shown by the following expression:

$$P_U = P_C + P_A \sin(2\pi f(t - t_0)) \quad (4)$$

where P_U is the transient acoustic pressure, P_C is the offset of the pressure-time curve, P_A is the amplitude, f is the frequency, and t_0 determines the initial phase of the pressure-time curve. t_0 was neglected because of the periodicity of the function. The exact values at different points are listed in Table 3. The sinusoidal equations all had negative offsets, and the frequencies were the same. The main differences were the acoustic pressure amplitude and the offset. A larger amplitude appeared at the pressure center point G, while the absolute value of the offset at point A was larger than that at point G in modes I and II. However, it was smaller at point A in mode III.

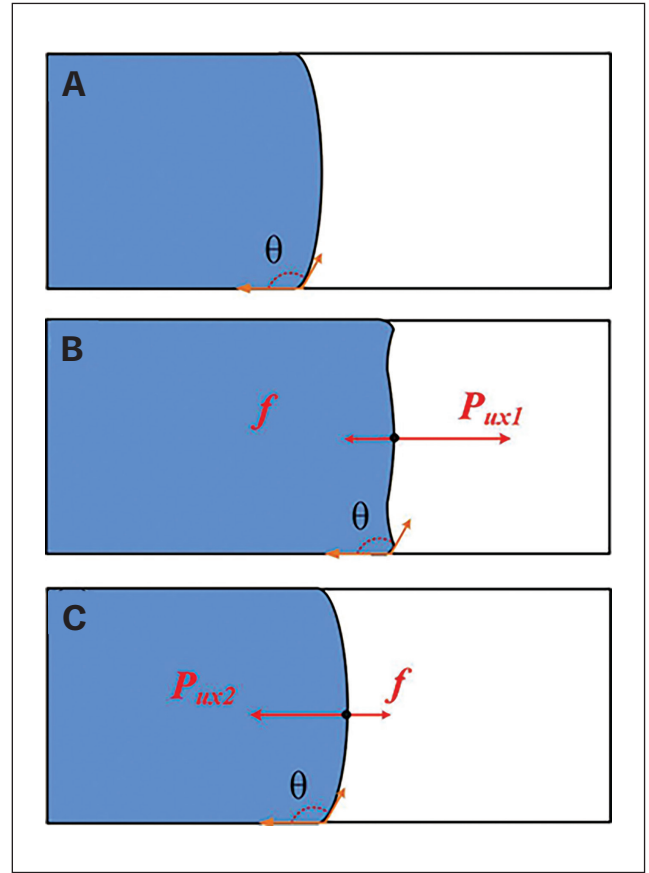


Fig. 11 – Physical model of the sonocapillary process within an acoustic cycle: A – Before ultrasonication; B – positive; C – negative forces in the X-direction.

The average acoustic pressure of an acoustic cycle can be calculated via integration:

$$\bar{P}_U = \frac{1}{T} \int_0^T P_C + P_A \sin(2\pi f(t - t_0)) dt = \frac{1}{T} \int_0^T P_C dt = P_C \quad (5)$$

Thus, the average was equal to the offset. The differences in the average acoustic pressure between points A and G for the three modes are shown in Fig. 9. In modes I and II, the average of the acoustic pressure at point A was smaller than that at point G. The differences were 12,200 and 6900 Pa, respectively. However, in mode III, the average acoustic pressure at point A was larger than that at point G, with a difference of approximately -1700 Pa.

Both the experimental results in Fig. 4 and the simulation results in Fig. 6 show the sonocapillary effect was realized in modes I and II, where the ultrasonication vibration could be transmitted to the lower substrate inside the joint clearance. Because the sonocapillary effect was the best in mode I, its filling velocity was calculated within a cycle, and the results are presented in Fig. 10. The filling morphology showed similar positive and negative variations to those of the acoustic pressure. The red and blue arrows in Fig. 10 represent the velocities of air and solder, respectively. The velocity changed with time. Combined with the results in Fig. 7, the solder velocity changes were sinusoidal. This caused the solder

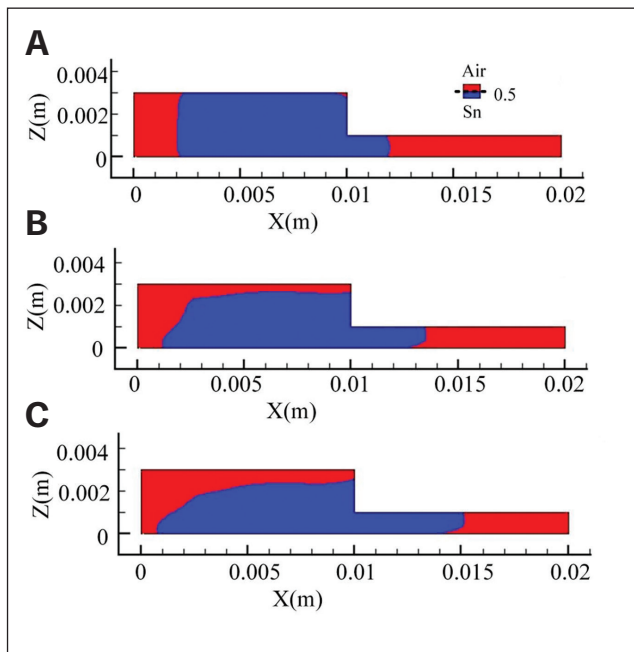


Fig. 12 — Filling morphologies under different ultrasonic amplitudes: A — 1 μm ; B — 5 μm ; C — 10 μm .

from points G to A to experience average movement to the joint clearance within an acoustic cycle. In other words, the liquid solder was sucked into the joint clearance by the larger negative pressure. Therefore, the sonocapillary effect was observed. However, the sonocapillary effect could not be observed in mode III.

Discussion

Physical Model of Sonocapillary Process

As previously discussed, the liquid solder experienced periodic movement caused by the pressure variations excited by the ultrasonic vibrations. With the passage of time, the solder was gradually forced into the joint clearance by the difference of the average pressure in the X-direction. The physical model of the sonocapillary process within an acoustic cycle is shown in Fig. 11. Before ultrasonication was applied, there was no driving force in the horizontal direction. The liquid solder remained static with a wetting angle of θ on the substrate — Fig. 11A.

Owing to the nonwettability of the liquid Sn on the 1060 Aluminum Alloy substrate, the wetting angle was more than 90 deg. However, when ultrasonication was applied, the balance state was broken, and an additional ultrasonic force with periodic sinusoidal variations appeared because of the pressure change. When the additional force in the X-direction, P_{ux1} , was positive (the positive direction was toward the joint clearance), the liquid solder moved into the joint clearance. The wetting angle was the same as before ultrasonication was applied, which can be observed in Fig. 4. At the same time, the resistance to the solder's advancement in the soldering

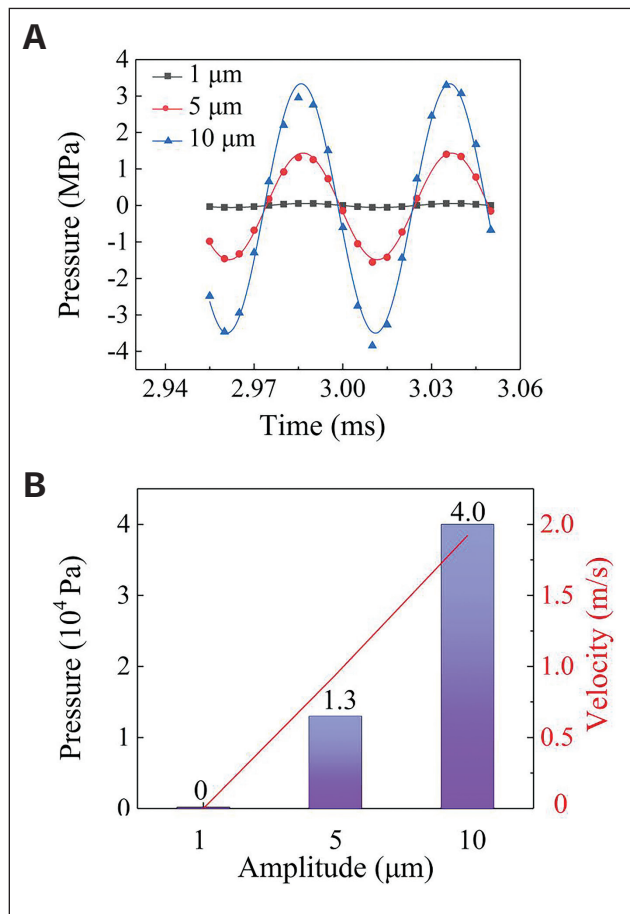


Fig. 13 — A — Acoustic pressure at the flowing front of point A; B — sonocapillary velocity and difference of average pressures of points A and G in joint clearances with different ultrasonic amplitudes.

joint clearance, f , occurred — Fig. 11B. In contrast, when the additional force P_{ux2} was negative, the fluid moved out of the joint clearance. The resistance to the solder's advancement in the soldering joint clearance changed its direction — Fig. 11C. However, as depicted in Table 2 and Fig. 9, the pressure change was not completely sinusoidal, and the average pressure of a cycle had a larger negative value at the filling front. At the same time, the influence of f also manifested. The liquid solder could not return to its initial position, and forward movement was realized within an acoustic cycle. Then, another acoustic pressure cycle occurred, and this process repeated itself. After a period of accumulation, the sonocapillary effect occurred.

Influence Parameters

Ultrasonic amplitude. The sonocapillary morphologies at 3 ms for different ultrasonic activation amplitudes are shown in Fig. 12. When the ultrasonic amplitude was set to 1 μm , the solder could not fill into the joint clearance. The filling distance was nearly 0.0015 m (0.059 in.) with an ultrasonic amplitude of 5 μm . When the ultrasonic amplitude increased to 10 μm , the filling distance increased to 0.003 m (0.118 in.). Details of the experimental verification of the influence of the

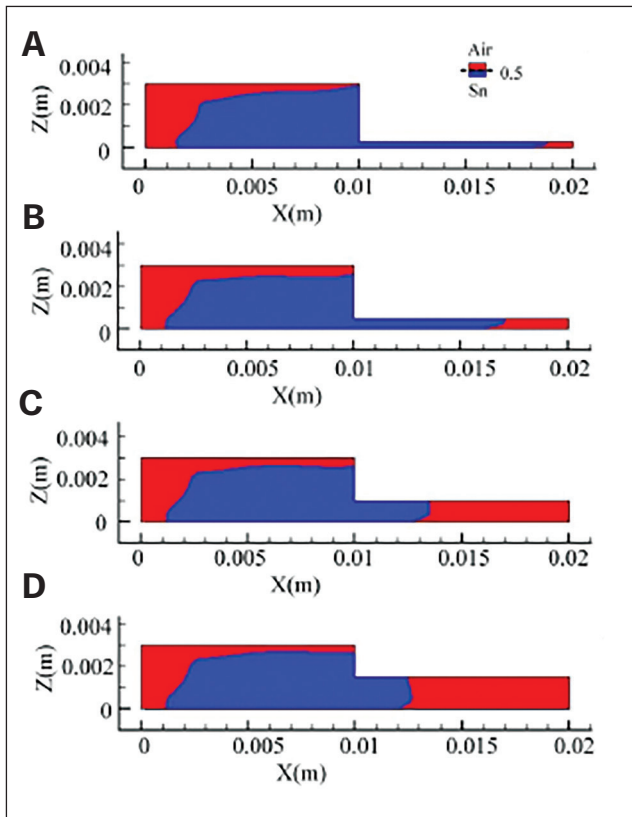


Fig. 14 – Sonocapillary morphologies of the liquid metal in joint clearances of different sizes: A – 0.3 mm; B – 0.5 mm; C – 1 mm; D – 1.5 mm.

ultrasonic amplitude on the sonocapillary morphology can be found in the authors' previous research (Ref. 24).

Figure 13A shows the change in the acoustic pressure at point A with the variation of the ultrasonic amplitude. When the ultrasonic amplitude was $1\ \mu\text{m}$, the acoustic pressure was very small. When the ultrasonic amplitude increased to $5\ \mu\text{m}$, the acoustic pressure was approximately 1.5 MPa. The highest pressure was 4 MPa when the ultrasonic amplitude was $10\ \mu\text{m}$. Larger ultrasonic amplitudes introduced more acoustic energy into the liquid solder; thus, the pressure increased. The differences in the average pressure between points A and G are shown in Fig. 13B. They exhibited the same variation trend with increasing ultrasonic amplitude. The average filling velocities in one vibration cycle, shown in Fig. 13B, were calculated via Equation 3. They increased sharply from 0 to 1.92 m/s when the ultrasonic amplitudes changed from 1 to $10\ \mu\text{m}$. Therefore, the sonocapillary length increased within 3 ms, as shown in Fig. 12.

Joint clearance width. The sonocapillary morphologies of the liquid metal in joint clearances of different sizes are shown in Fig. 14. The filling time was 3 ms. When the joint clearance width was 0.3 mm (0.011 in.), the liquid metal moved forward 0.007 m (0.275 in.), and the largest filling distance was observed. In addition, the filling distance showed a decreasing trend with increasing joint clearance size (i.e., 0.005 m [0.196 in.] in the joint clearance with a width of 0.5 mm [0.019 in.]). The sonocapillary length was less than 0.002 m (0.078 in.) in the joint clearance with a

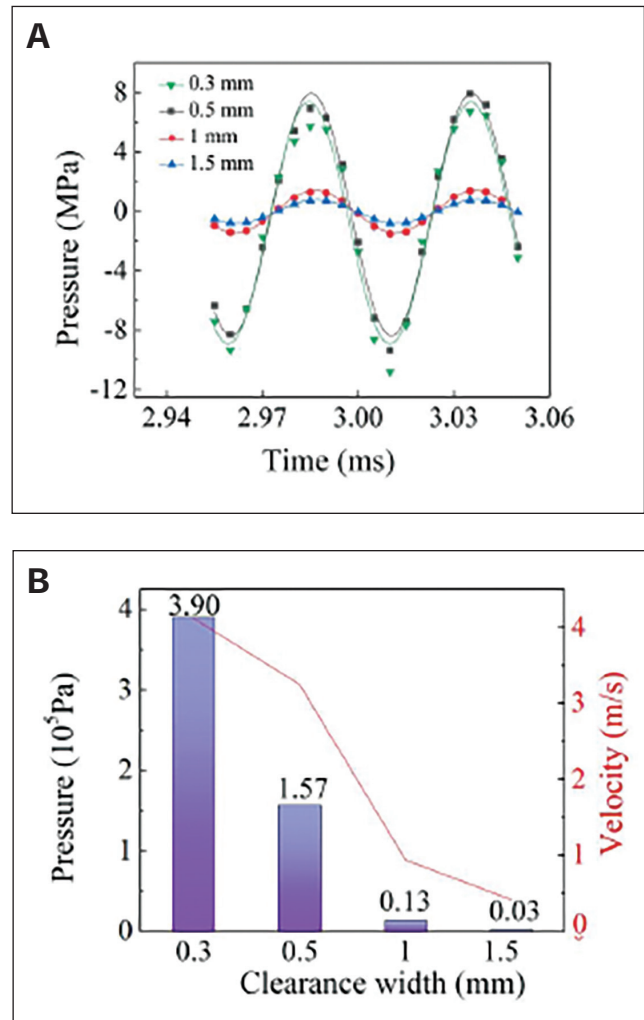


Fig. 15 – A – Acoustic pressure at the flowing front of point A; B – sonocapillary velocity and the difference of average pressures of points A and G in joint clearances of different widths.

width of 1 mm. Upon increasing the joint clearance size to 1.5 mm (0.059 in.), no evident filling was observed in 3 ms. These simulation results agreed with those reported in the authors' previous work (Ref. 24), which showed that a larger joint clearance width led to a smaller sonocapillary velocity.

With the increasing joint clearance width, the acoustic pressure sharply decreased, a point that was reported in the authors' previous work (Ref. 27). As shown in Fig. 15A, the pressure amplitude was as high as 8 MPa in the joint clearances with widths of 0.3 and 0.5 mm. The acoustic pressure was below 2 MPa when the joint clearance width increased to 1 and 1.5 mm. A similar decreasing trend occurred in the differences of the average pressure with increasing joint clearance width. Meanwhile, the sonocapillary driving force decreased. Thus, the average sonocapillary velocity near 3 ms at point A changed from 4.12 to 0.42 m/s – Fig. 15B. It was also found in several other works that the infiltration velocity decreased with the increasing joint clearance width (Ref. 28). Therefore, by obtaining a better sonocapillary effect in the ultrasonic-assisted soldering of hard-to-wet materials, the joint clearance width should be decreased.

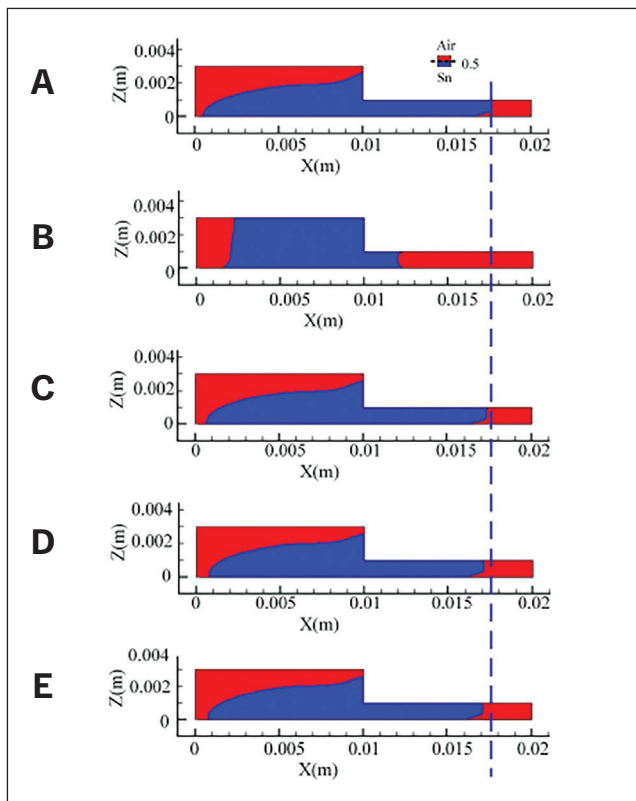


Fig. 16 – Filling morphologies of solder with different wetting angles on 1060 Aluminum Alloy: A – 30 deg with ultrasonication; B – 30 deg without ultrasonication; C – 90 deg with ultrasonication; D – 130 deg with ultrasonication; E – 180 deg with ultrasonication.

Wetting angle. Figure 16 presents the sonocapillary morphologies of the solder with different wetting angles on 1060 Aluminum Alloy substrate and the filling state with a wetting angle of 30 deg without ultrasonication. The wetting angles were set at 30, 90, 130, and 180 deg, and the wetting time was 6 ms. The biggest filling length was obtained when the wetting angle was 30 deg and with ultrasonication. However, the filling length was extremely small for the same filling time of a 30-deg wetting angle without ultrasonication. It was predicted by the current simulation that ultrasonic-driven flow is much faster than surface tension-driven flow when the contact angle is small. With decreasing wettability of the solder on the substrate, the sonocapillary length showed a slight decreasing trend. The longest sonocapillary length, obtained when the wetting angle was 30 deg, was only approximately 0.0005 m (0.019 in.) longer than the shortest one (obtained when the wetting angle was 180 deg), indicating that the wettability of the solder on the substrate had a smaller influence on the sonocapillary effect. This point is demonstrated in Fig. 4, which shows that sonocapillary was realized before wetting. Thus, ultrasonic-assisted soldering can be used to join several hard-to-wet materials, such as aluminum nitride (AlN) (Ref. 29) and SiC (Ref. 30). Moreover, the soldering process can be independent of the wettability.

The acoustic pressure and filling velocity at the flowing front as well as the difference of average pressure at the

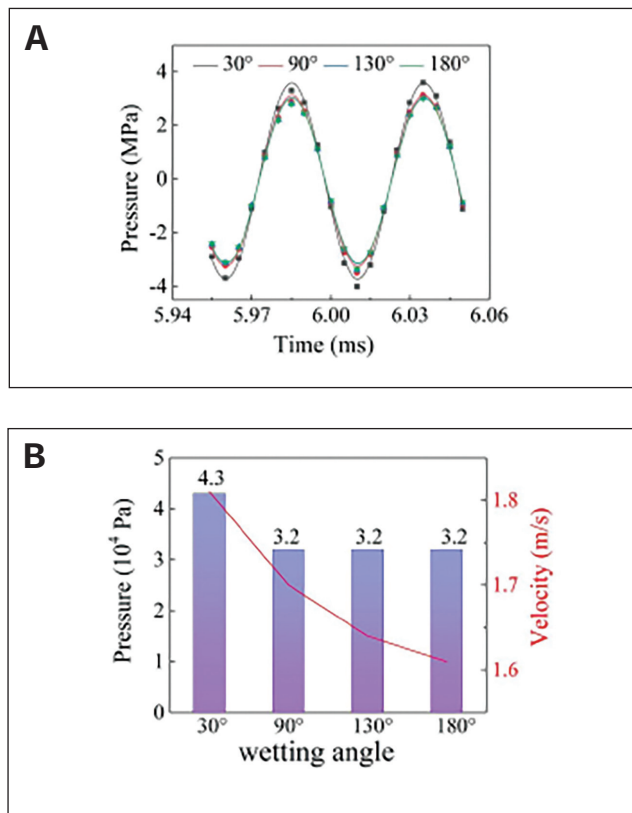


Fig. 17 – A – Acoustic pressure at the flowing front of point A; B – sonocapillary velocity and the difference of average pressure of points A and G for different wetting angles on the 1060 Aluminum Alloy substrate.

wpressure center and the filling front for different wetting angles are shown in Fig. 17. The pressure and time curves were almost the same. The differences of acoustic pressure between the pressure center and filling front were approximately 4.3×10^4 Pa (wetting angle of 30 deg) and 3.2×10^4 Pa (wetting angles of 90, 130, and 180 deg). The sonocapillary velocity varied from 1.81 to 1.61 m/s – Fig. 17B. In general, the influence of the wetting conditions on the sonocapillary effect was not as significant as that of the joint clearance width or the ultrasonic amplitude. Therefore, the wettability of the solder on the substrate is not a prerequisite for ultrasonic-assisted soldering, which has been demonstrated in several other works (Refs. 7, 8).

Base material. Figure 18 shows the sonocapillary effect of liquid solder for different base materials. The base materials were chosen as 1060 Aluminum, 5056 Aluminum, and Fe36Ni Alloys, which was the same as those in the publication (Ref. 24). The filling time was 3 ms. As reported in previous work (Ref. 24), the stiffness between 1060 and 5056 Aluminum Alloys was very similar. Thus, the sonocapillary length was without obvious variation. But the filling length was much bigger in Fig. 18C than those in Figs. 18A and B due to the high stiffness of the Fe36Ni Alloy.

The acoustic pressure at the flowing front of point A, the sonocapillary velocity, and the difference of average pressure of points A and G for different base materials are presented in Fig. 19. The acoustic pressure was the biggest on the Fe36Ni

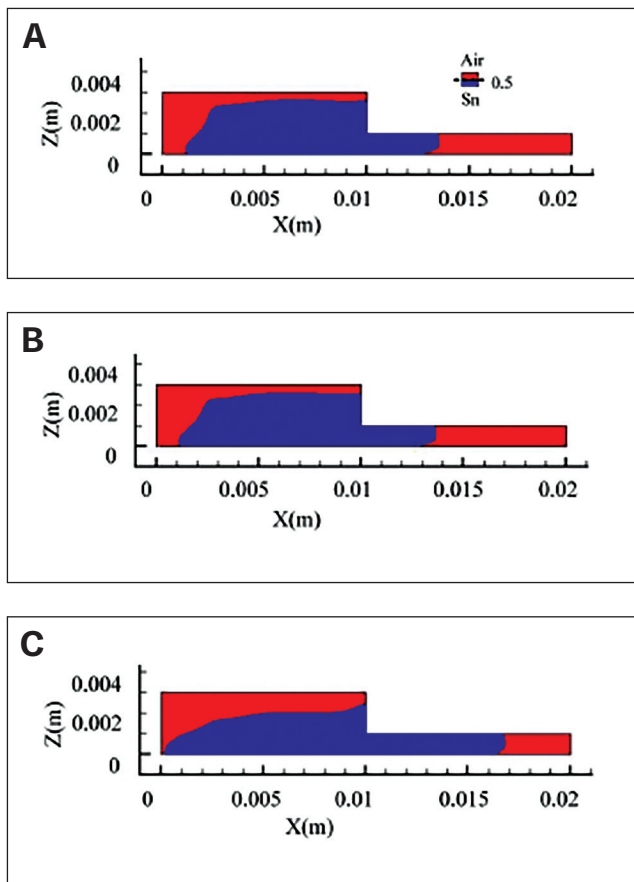


Fig. 18 – Filling morphologies of solder for different materials: A – 1060; B – 5056 Aluminum Alloy; C – Fe36Ni Alloy.

Alloy, with an amplitude of approximately 6 MPa. On the two aluminum alloys, the pressure and time curves were almost the same. The acoustic pressure amplitudes were less than 2 MPa. In Fig. 19B, the sonocapillary velocity and the difference of the average pressure of points A and G also showed a similar variation trend to the acoustic pressure among the three base materials. The high stiffness in the base material caused a better sonocapillary effect. This simulation result agreed well with the experimental results in one of the authors' previous works (Ref. 24).

Conclusions

1) Both simulations and experiments indicated that the sonocapillary effect occurred when vibrations could be transmitted to the lower substrate inside the joint clearance. The best sonocapillary effect was achieved under the condition where the entire lower substrate was vibrated. However, the sonocapillary effect could not be realized when ultrasonication was only limited to the lower substrate outside the joint clearance.

2) An acoustic pressure with sinusoidal features was produced in the liquid solder by the vibrations caused by ultrasonication on the lower substrate in the simulation model.

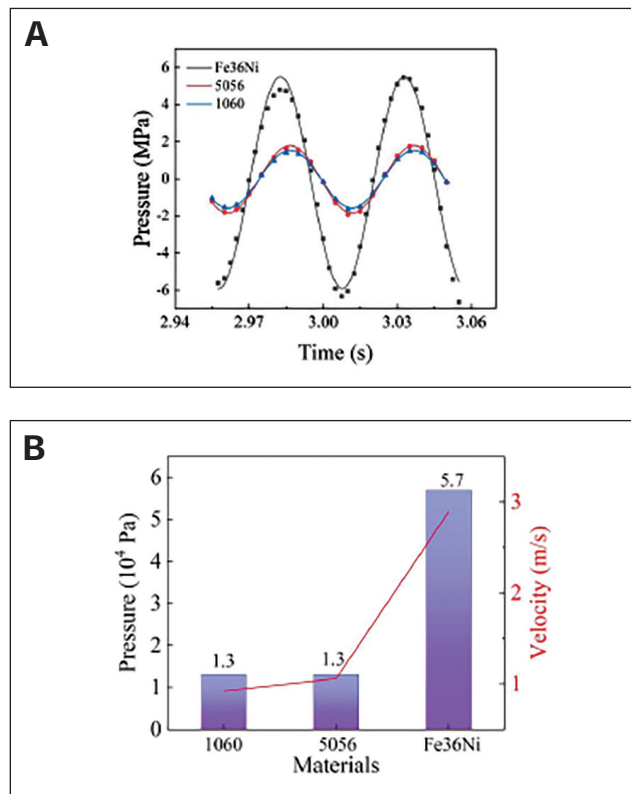


Fig. 19 – A – Acoustic pressure at the flowing front of point A; B – sonocapillary velocity and the difference of average pressure of points A and G for different base materials.

3) Based on the simulation model, the sonocapillary effect was forced by the average pressure difference in the horizontal direction, and the liquid solder was sucked into the joint clearance by the larger negative pressure.

Acknowledgment

This project was supported by the National Natural Science Foundation of China (No. 51574099).

References

- Or, D., and Tuller, M. 2005. "Capillarity." In *Encyclopedia of Soils in the Environment*, edited by Hillel, D., 155–164. Cambridge, Mass.: Academic Press.
- Wang, Y., Ho, C., and Tsai, H. L. 2010. Effect of in addition on wetting properties of Sn-Sn-Sn/Cu soldering. *Materials Transactions* 51(9): 1735–1740. DOI: 10.2320/matertrans.MJ201004
- Chen, B., Xiong, H., Cheng, Y., Mao, W., and Wu, S. 2015. Microstructure and property of AlN joint brazed with Au-Pd-Co-Ni-V brazing filler. *Journal of Materials Science & Technology* 31(10): 1034–1038. DOI: 10.1016/j.jmst.2014.11.026
- Ji, Y., Fu, R., Lv, J., Zhang, X., Chen, X., Li, G., and Liu, X. 2020. Enhanced bonding strength of Al₂O₃/AlN ceramics joined via glass frit with gradient thermal expansion coefficient. *Ceramics International* 46(8): 12806–12811. DOI: 10.1016/j.ceramint.2020.02.050
- Xu, Z., Yan, J., Wu, G., Kong, X., and Yang, S. 2005. Interface structure and strength of ultrasonic vibration liquid phase bonded joints of Al₂O₃p/6061Al composites. *Scripta Materialia* 53(7): 835–839. DOI: 10.1016/j.scriptamat.2005.06.009

6. Chen, X., Xie, R., Lai, Z., Liu, L., Zou, G., and Yan, J. 2016. Ultrasonic-assisted brazing of Al-Ti dissimilar alloy by a filler metal with a large semi-solid temperature range. *Materials and Design* 95: 296–305. DOI: 10.1016/j.matdes.2016.01.109
7. Xu, Z., Ma, L., Yan, J., Yang, S., and Du, S. 2012. Wetting and oxidation during ultrasonic soldering of an alumina reinforced aluminum-copper-magnesium (2024 Al) matrix composite. *Composites Part A: Applied Science & Manufacturing* 43(3): 407–414. DOI: 10.1016/j.compositesa.2011.12.006
8. Xu, Z., Li, Z., Qi, Y., and Yan, J. 2019. Soldering porous ceramics through ultrasonic-induced capillary action and cavitation. *Ceramics International* 45(7): 9293–9296. DOI: 10.1016/j.ceramint.2019.01.171
9. Mason, J., Chemat, F., and Vinatoru, M. 2011. The extraction of natural products using ultrasound or microwaves. *Current Organic Chemistry* 15(2): 237–247. DOI: 10.2174/138527211793979871
10. Mittal, R., Tavanandi, H. A., Mantri, V. A., and Raghavarao, K. 2017. Ultrasound assisted methods for enhanced extraction of Phycobiliproteins from marine macro-algae, *Gelidium pusillum* (Rhodophyta). *Ultrasonics Sonochemistry* 38: 92–103. DOI: 10.1016/j.ultsonch.2017.02.030
11. Chemat, F., Rombaut, N., Sicaire, A. G., Meullemiestre, A., Fabiano-Tixier, A., and Abert-Vian, M. 2016. Ultrasound assisted extraction of food and natural products. Mechanisms, techniques, combinations, protocols and applications. A Review. *Ultrasonics Sonochemistry* 34: 540–560. DOI: 10.1016/j.ultsonch.2016.06.035
12. Eskin, G. I. 2001. Broad prospects for commercial application of the ultrasonic (cavitation) melt treatment of light alloys. *Ultrasonics Sonochemistry* 8(3): 319–325. DOI: 10.1016/S1350-4177(00)00074-2
13. Naderi, K., and Babadagli, T. 2010. Influence of intensity and frequency of ultrasonic waves on capillary interaction and oil recovery from different rock types. *Ultrasonics Sonochemistry* 17(3): 500–508. DOI: 10.1016/j.ultsonch.2009.10.022
14. Sritharan, K., Strobl, C. J., Schneider, M. F., Wixforth, A., and Guttenberg, Z. 2006. Acoustic mixing at low Reynold's numbers. *Applied Physics Letters* 88: 054102. DOI: 10.1063/1.2171482
15. Wixforth, A., Strobl, C., Gauer, C., Toegl, A., Scriba, J., and Guttenberg, Z. V. 2004. Acoustic manipulation of small droplets. *Analytical and Bioanalytical Chemistry* 379: 982–991. DOI: 10.1007/s00216-004-2693-z
16. Cecchini, M., Girardo, S., Pisignano, D., Cingolani, R., and Beltram, F. 2008. Acoustic-counterflow microfluidics by surface acoustic waves. *Applied Physics Letters* 92: 104103. DOI: 10.1063/1.2889951
17. Malykh, N., Petrov, V., and Sankin, G. 2003. On sonocapillary effect. *Proceedings of the 5th World 26 Congress on Ultrasonics (WCU)*: 1343–1346.
18. Dezhkunov, N. V., and Leighton, T. G. 2004. Study into correlation between the ultrasonic capillary effect and sonoluminescence. *Journal of Engineering Physics and Thermophysics* 77(1): 53–61. DOI: 10.1023/B:JOEP.0000020719.33924.aa
19. Rozina, Yu E. 2002. Effect of pulsed ultrasonic field on the filling of a capillary with a liquid. *Colloid Journal* 64(3): 359–363. DOI: 10.1023/A:1015929011920
20. Lang, R. J. 1962. Ultrasonic atomization of liquids. *The Journal of the Acoustic Society of America* 34: 6–8. DOI: 10.1121/1.1909020
21. Dezhkunov, N. V., and Prokhorenko, P. P. 1980. Action of ultrasound on the rise of a liquid in a capillary tube and its dependence on the properties of the liquid. *Journal of Engineering Physics* 39(3): 1014–1019. DOI: 10.1007/BF00825930
22. Tamura, S., and Hatakeyama, M. 2013. The role of acoustic cavitation in liquid pressurization in narrow tubes. *Journal of Applied Physics* 113(14): 144905. DOI: 10.1063/1.4801422
23. Hu, J., Tan, C., and Hu, W. 2007. Ultrasonic microfluidic transportation based on a twisted bundle of thin metal wires. *Sensors and Actuators A* 135: 811–817. DOI: 10.1016/j.sna.2006.10.007
24. Xu, Z., Li, Z., Ma, L., Cao, Z., and Yan, J. 2019. Dynamic behavior of solder filling during ultrasonic soldering. *Welding Journal* 98(7): 194-s to 203-s. DOI: 10.29391/2019.98.017
25. Li, Z., Xu, Z., Ma, L., Wang, S., Liu, X., and Yan, J. 2019. Cavitation at filler metal/substrate interface during ultrasonic-assisted soldering. Part II: Cavitation erosion effect. *Ultrasonics Sonochemistry* 50: 278–288. DOI: 10.1016/j.ultsonch.2018.09.027
26. Ma, L., Xu, Z., Zheng, K., Yan, J., and Yang, S. 2014. Vibration characteristics of aluminum surface subjected to ultrasonic waves and their effect on wetting behavior of solder droplets. *Ultrasonics* 54(3): 929–937. DOI: 10.1016/j.ultras.2013.11.005
27. Li, Z., Xu, Z., Ma, L., Wang, S., Liu, X., and Yan, J. 2018. Cavitation at filler metal/substrate interface during ultrasonic-assisted soldering. Part I: Cavitation characteristics. *Ultrasonics Sonochemistry* 49: 249–259. DOI: 10.1016/j.ultsonch.2018.08.009
28. Zhao, W., Yan, J., Yang, W., and Yang, S. 2008. Capillary filling process during ultrasonically brazing of aluminium matrix composites. *Science and Technology of Welding and Joining* 13(1): 66–69. DOI: 10.1179/174329308X271742
29. Chen, S., Xu, Z., Li, Z., Ma, Z., Zhang, M., Lu, Y., and Yan, J. 2022. Ultrasonic-assisted wetting and soldering of AlN ceramic by using a nonactive solder (Sn9Zn) in air. *Ceramics International* 48(2): 1898–1907. DOI: 10.1016/j.ceramint.2021.09.274
30. Wu, B., Guo, W., He, J., Xiu, Z., and Yan, J. 2018. Microstructure evolution of SiC/SiC joints during ultrasonic-assisted air bonding using a Sn–Zn–Al alloy. *Ceramics International* 44(2): 1284–1290. DOI: 10.1016/j.ceramint.2017.07.169

SHU CHEN, ZHIWU XU (xuzw@hit.edu.cn), **ZHENGWEI LI** (lizhengwei@hit.edu.cn), **ZHONGWEI MA, LIN MA, and JIUCHUN YAN** are with the State Key Laboratory of Advanced Welding and Joining, Harbin Institute of Technology, Harbin, China.